

391 ESTIMATING THE ANNUAL AND SEASONAL DIURNAL CYCLE OF PRECIPITATION OVER CENTRAL FLORIDA USING WSR-88D RADAR AND TIPPING BUCKET RAIN GAUGE DATA

J. L. Pippitt^{1,2,*}, D. B. Wolff^{1,2}, and D. A. Marks^{1,2}
1 NASA Goddard Space Flight Center, Greenbelt, Maryland
2 Science Systems & Applications, Inc, Lanham, Maryland

1. INTRODUCTION

Decade-long radar and rain gauge data sets from multiple ground validation sites have allowed detailed analyses of diurnal rainfall cycles and seasonal rain rates from various climatological regimes. Site-specific diurnal rainfall analysis provide observations of local rainfall patterns, daily rainfall maximum and minimum cycles, and terrain-influenced rates and coverage; all of which benefit climatological, precipitation modeling and forecasting, algorithm development, and data assimilation studies. Several recent diurnal rainfall studies such as Sorooshian et al. (2002) have focused on the large scale diurnal cycle, as estimated by satellites such as NASA's Tropical Rainfall Measuring Mission (TRMM). However, our approach is focused over smaller areas (0.25° x 0.25°), with near round-the-clock sampling via ground-based radars and several networks of tipping bucket rain gauges. We observed the decade-long (2000-2009) annual and seasonal diurnal cycles of rainfall over quarter degree pixels using quality controlled gauge and radar data from the TRMM Ground Validation (GV) radar site at Melbourne, Florida (MELB). The MELB rainfall coverage area is centered on the KMLB WSR-88D radar located at 28.1°N, 80.6°W. Seventy percent of MELB's annual rainfall occurs between June and September. A large majority of the rainfall is due to sea-breeze-induced isolated convective systems and large organized tropical storms. MELB also receives a contribution from mid latitude synoptic systems during Northern Hemispheric winter months when frontal boundaries occasionally affect MELB weather (Wolff et al. 2005).

Two data sets, radar data and gauge data, were evaluated and compared to assess the annual and seasonal diurnal cycle of precipitation. Instantaneous rain rates from the radar were obtained from the TRMM Satellite Validation Office

(TSVO) 2A-53 product from 2000-2009. These rates are determined by comparison of radar reflectivity and rain gauge data via the Probability Matching Method (PMM - Rosenfeld et al 1994). The 2A-53 product has a 151 x 151 km² coverage area with 2 km horizontal resolution. Gauge rain rates were obtained from the 2A-56 product from 2000-2009. Wolff et al. (2005) provide a detailed description of all TSVO products. Our method is limited to quarter degree pixels that contain gauges. To present our data we grouped each pixel into three specific geographical regions: coastal, mid-range, and inland (Figure 1). The diurnal cycle of each region was determined by calculating the mean of all the pixels within that group. The resultant diurnal cycle allowed us to analyze each regions time of maximum and minimum rain intensity tmax and tmin, their corresponding rain rate intensity rmax and rmin, and other significant secondary modes. Our approach gave us an annual and seasonal understanding of how the daily cycle of rainfall differs for each region and what meteorological factors are involved.

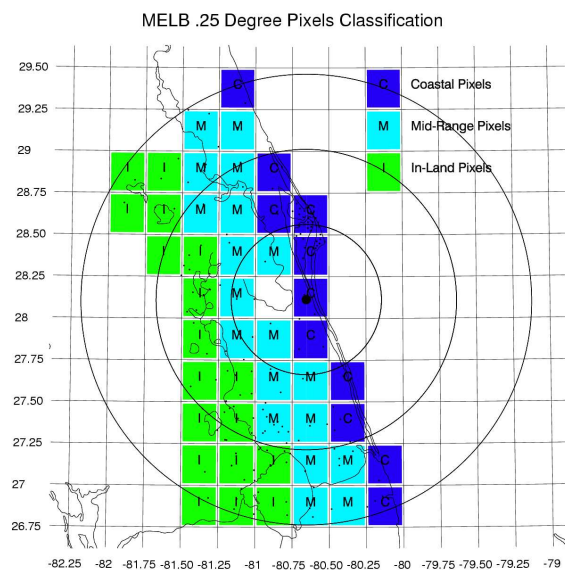


Figure 1. Map of MELB quarter degree (27 km²) pixels that contain rain gauges and their regional classification. Dots represent gauge locations.

* Corresponding author address: Jason L. Pippitt, TRMM Satellite Validation Office, NASA Goddard Space Flight Center, Code 613.1 Greenbelt, MD 20771; e-mail: Jason.L.Pippitt@nasa.gov

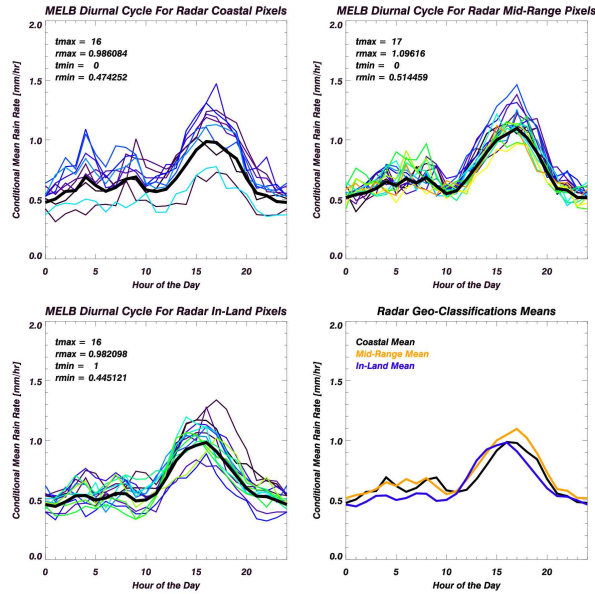


Figure 2. The annual diurnal cycle of conditional mean rain rate using radar data for the three geographical regions. The bold lines are the average of all the pixels in a given region, and are compared in the bottom right panel. These statistics were derived from the 2A-53 rain rate product over a ten year period from 2000-2009.

2. ANNUAL DIURNAL CYCLE

On an annual basis, t_{max} for all regions, and both radar and gauge data sets, occurs in the afternoon (Figures 2 and 3). Analysis of t_{max} reveals that coastal pixels have the earliest maximums. Precipitation starts near the coast, and as it moves west it fully matures one hour later over mid-range pixels. Similar landward phase propagation has been noted for coastal regimes most recently by Kikuchi et al. (2007). For both data sets mid-range pixels have the highest r_{max} values. When cooler air over the ocean advects inland and meets warmer air over land a convergence zone forms, our data suggest this zone is most prevalent over mid-range pixels. In mid-range pixels r_{max} values are 10.6% higher than coastal pixels and 11.0% higher than inland pixels for radar data and 4.9% higher than coastal pixels and 7.8% higher than inland pixels for gauge data. Mid-range pixels clearly have the highest rain rates annually than the other two regions. For all regions and all data sets t_{min} occurs around midnight when the boundary layer is the most stable. Maritime convection develops after midnight due to gravity waves emitted by land heating (Mapes et al. 2002). These showers move

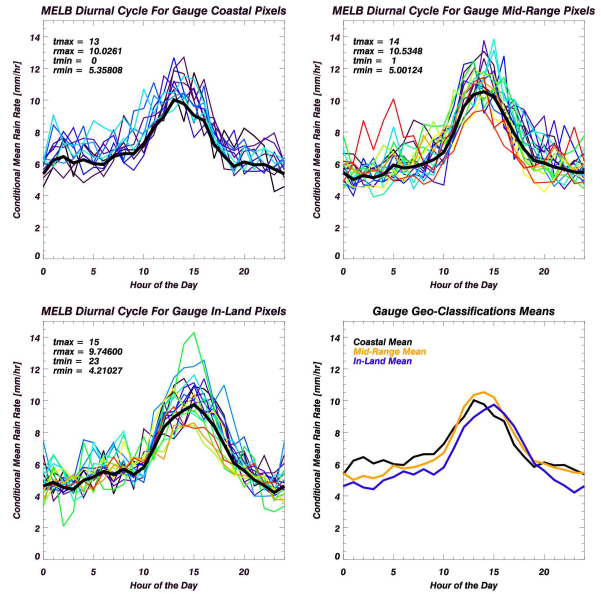


Figure 3. The annual diurnal cycle of conditional mean rain rate using gauge data for the three geographical regions. The bold lines are the average of all the pixels in a given region, and are compared in the bottom right panel. These statistics were derived from the 2A-56 rain gauge product over a ten year period from 2000-2009.

toward the coast and contribute to a small early-morning mode that is evident in both data sets. Maritime showers have less of an effect on inland pixels, thus they have the lowest r_{min} values. Further contributions to the early morning and late morning modes are discussed in our seasonal analysis where these modes are more pronounced.

3. SUMMER DIURNAL CYCLE

During the summer months (June – August), for all regions and all data sets t_{max} occurs in the afternoon, which, given its magnitude also dominates the annual cycle (Figures 4 and 5). Coastal pixels have the highest r_{max} for gauge data whereas r_{max} for radar data is highest for mid-range pixels. A strong sea breeze and intense inland heating during the summer months would imply that the convergence zone establishes itself between mid-range and inland pixels. This pattern is evident in the radar data where mid-range pixels have the highest r_{max} values followed by inland pixels. The lack of a dense rain gauge network over inland pixels may be skewing the gauge data results; however, the radar data conveys the presence of a relatively robust summer cycle. The

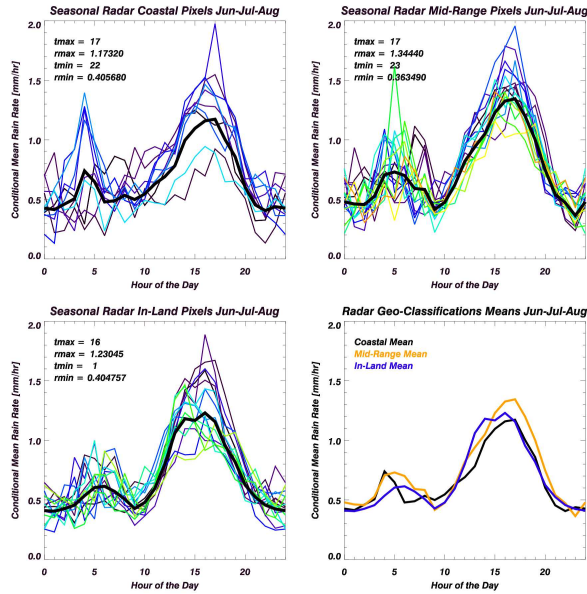


Figure 4. The summer diurnal cycle of conditional mean rain rate using radar data for the three geographical regions. The bold lines are the average of all the pixels in a given region, and are compared in the bottom right panel. These statistics were derived from the 2A-53 rain rate product over a ten year period from 2000-2009.

radar data suggests that the mid-range pixels rmax values are 13.6% higher than coastal pixels and 8.9% higher than inland pixels, and thus clearly the area with peak rain rates. Coastal pixels have the earliest tmin, as precipitation dissipates earlier over the coast where less intense convection occurs. In both data sets a secondary mode is evident in the morning hours. The time shift between each regions secondary mode suggests that showers initiate over the ocean and move inland during the overnight to morning hours. Winds are weak during the overnight hours allowing precipitation to move toward the west. The similarities between the annual and summer cycles confirm the dominant season for MELB is the summer.

4. AUTUMN DIURNAL CYCLE

During the autumn months (September – November), tmax occurs in the afternoon for all regions and all data sets (Figures 6 and 7). Mid-range pixels have the highest rmax values, suggesting the convergence zone is prevalent in this region. Sea-breeze and day time heating decrease during autumn thus allowing the convergence zone to move closer to the coast, as

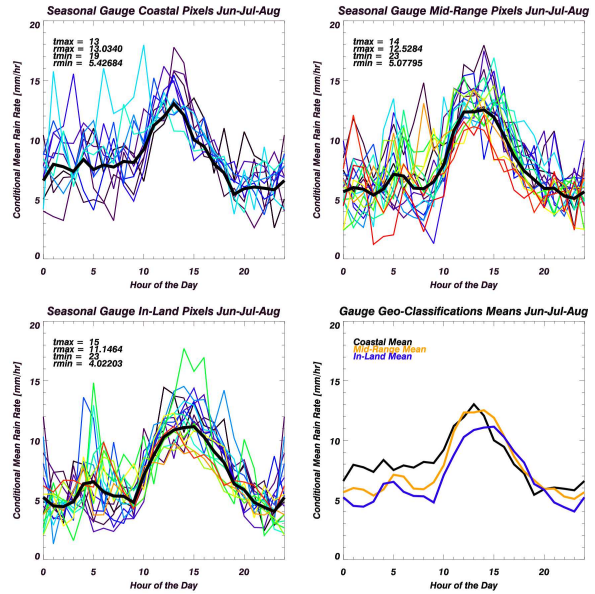


Figure 5. The summer diurnal cycle of conditional mean rain rate using gauge data for the three geographical regions. The bold lines are the average of all the pixels in a given region, and are compared in the bottom right panel. These statistics were derived from the 2A-56 rain gauge product over a ten year period from 2000-2009.

suggested by the radar data having the highest rmax for mid-range pixels followed by coastal pixels. Mid-range pixels rmax values are 2.8% higher than coastal pixels and 7.0% higher than inland pixels for radar data, 11.9% higher than coastal pixels and 8.2% higher than inland pixels for gauge data. For all regions and all data sets tmin occurs around midnight. A secondary mode occurs during the overnight to morning hours and is caused by maritime convection that moves inland and is heaviest near the coast. We found the secondary mode to be most pronounced during autumn, similar to findings of Yang et al. (2006). Comparatively, the afternoon mode found in the radar data for mid-range pixels is 19.7% higher than the secondary mode, thus establishing itself as the dominate mode, although the autumnal secondary mode does influence the annual cycle's early and late morning modes.

5. WINTER DIURNAL CYCLE

Gauge data is extremely noisy during the winter months (December – February) due to the relatively small amount of rainfall during this period (Figure 9). For gauge data tmax is in the afternoon and tmin occurs around midnight; rmax

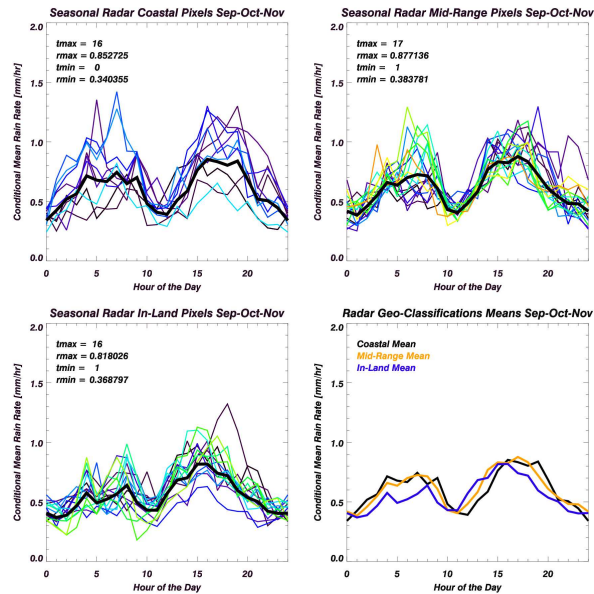


Figure 6. The autumn diurnal cycle of conditional mean rain rate using radar data for the three geographical regions. The bold lines are the average of all the pixels in a given region, and are compared in the bottom right panel. These statistics were derived from the 2A-53 rain rate product over a ten year period from 2000-2009.

values for the regions only differ by 3%. Radar data conveys a different pattern than gauge data, showing a morning r_{max} with coastal pixels having the highest values and rain rates substantially decreasing as you move inland (Figure 8). The morning winter maximum was also found in Yang et al. (2006) and Roy et al. (2005). Furthermore, Schwartz et al. (1979) conveys the source of the morning maximum to be a winter quasi-stationary front that routinely sets up within this area and is associated with convective precipitation. Coastal pixels r_{max} values are 4.9% higher than mid-range pixels and 30.1% higher than inland pixels. Land sea interactions are weak during the winter, only affecting areas close to the coast, thus in-land rain rates are dramatically lower than coastal rain rates. Two minimums are observed, one during the early morning (approximately 0600 LT) and one in the afternoon (approximately 1600 LT). Three modes are evident with the largest occurring during the morning (approximately 0900 LT), and two secondary modes, occurring overnight (approximately 0200 LT) and one during the evening (approximately 1900 LT). The evening secondary mode is influenced by sea-breeze induced showers that occur during warm winter days. The overnight mode can be attributed to

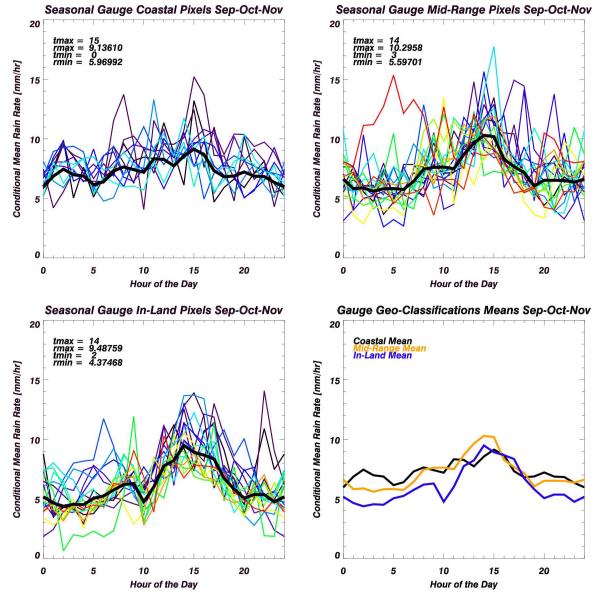


Figure 7. The autumn diurnal cycle of conditional mean rain rate using gauge data for the three geographical regions. The bold lines are the average of all the pixels in a given region, and are compared in the bottom right panel. These statistics were derived from the 2A-56 rain gauge product over a ten year period from 2000-2009.

nocturnal maritime convection that develops occasionally during the winter. The morning mode for coastal pixels is 35.1% higher than the two secondary modes. The annual cycle late morning mode is primarily influenced by the high amplitude winter morning rainfall maximum portrayed in the radar data, with autumn contributing to a lesser extent. The differences in radar and gauge data can be attributed to the sporadic and relatively light nature of precipitation during the winter, sampling issues pertaining to radar data sampling the entire 27 km² grid versus point measurements within that grid for gauge data, and the sparseness of gauge data as you move inland.

6. SPRING DIURNAL CYCLE

An afternoon t_{max} occurs for all regions and all data sets during the spring months (March – May) (Figures 10 and 11). Radar data implies that r_{max} values for mid-range pixels are 10.1% higher than coastal pixels and 16.5% higher than inland pixels, whereas gauge data coastal pixels have the highest r_{max} values and are only 0.1% higher than mid-range pixels and 1.3% higher than inland pixels. Gauge data suggests that rainfall is uniform over the region during the spring, while

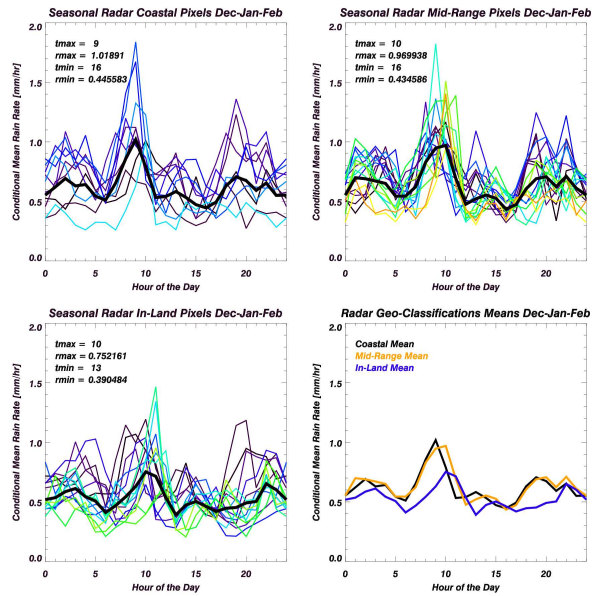


Figure 8. The winter diurnal cycle of conditional mean rain rate using radar data for the three geographical regions. The bold lines are the average of all the pixels in that region, and are compared in the bottom right panel. These statistics were derived from the 2A-53 rain rate product over a ten year period from 2000-2009.

radar data suggests mid-range pixels have a substantially higher rmax. Even with this difference we can discern that the convergence zone during the spring sets up over mid-range and coastal pixels because these two regions have the highest rmax values. The increase in daytime heating brings the sea breeze convergence zone farther inland. Coastal pixels have the latest tmin for both data sets. Nocturnal maritime convection contributes first to this area, consequently increasing rain rates, while the other two regions are still experience falling rain rates thus leading to later tmin's. Mid-range and coastal pixels have the highest rmin values. Intense convection over these areas never fully dissipates when nocturnal convection begins, rmin does not fall as low as inland pixels. A small morning mode is evident in the radar data. This mode shows precipitation beginning to the east, increasing over mid-range pixels, and then dissipating over inland pixels. The spring secondary mode is the only season showing showers increasing in intensity as they move over mid-range pixels. Nighttime inversions over this area may contribute to enhanced rain rates for the morning mode (Schwartz et al. 1979). The most influential aspect of spring on the annual cycle is the large afternoon maximum.

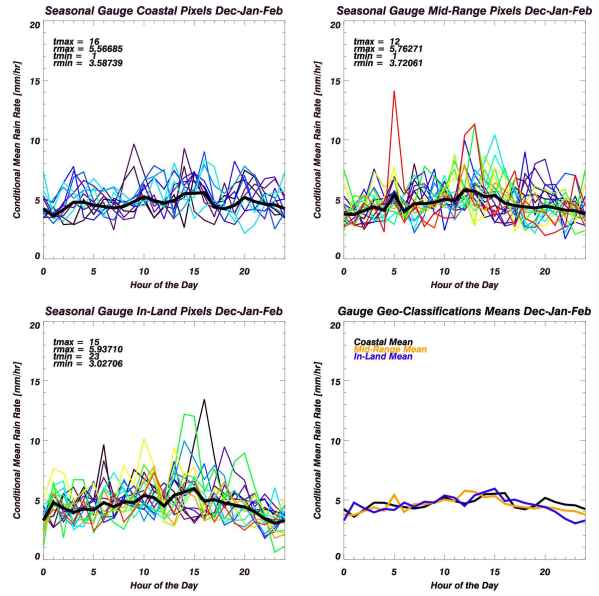


Figure 9. The winter diurnal cycle of conditional mean rain rate using gauge data for the three geographical regions. The bold lines are the average of all the pixels in a given region, and are compared in the bottom right panel. These statistics were derived from the 2A-56 rain gauge product over a ten year period from 2000-2009.

7. SUMMARY

The availability of high resolution high quality radar and gauge data have provided the opportunity to analyze the seasonal diurnal cycle of rain rates on a relatively small spatial scale ($0.25^\circ \times 0.25^\circ$). Spring, summer, and autumn have similar phases as the annual cycle with an afternoon maximum and a nighttime minimum. Winter has a different phase, with a maximum occurring in the late morning hours and a minimum occurring in the afternoon hours (Figures 12 and 13). This phase difference may be attributed to a winter quasi-stationary front that routinely sets up over MELB and is associated with convective precipitation (Schwartz et al. 1979). The area of maximum rainfall is closest to the coast during the winter the weakest, and furthest inland during the summer months when these factors are the strongest. Summer has the highest amplitude followed by spring, autumn and winter, thus summer months have the greatest influence on the annual cycle (Figures 12 and 13), and indeed on the annual rainfall budget. The relatively high amplitude of the radar data winter maximum suggests that it is a strong influence on the annual cycle's late

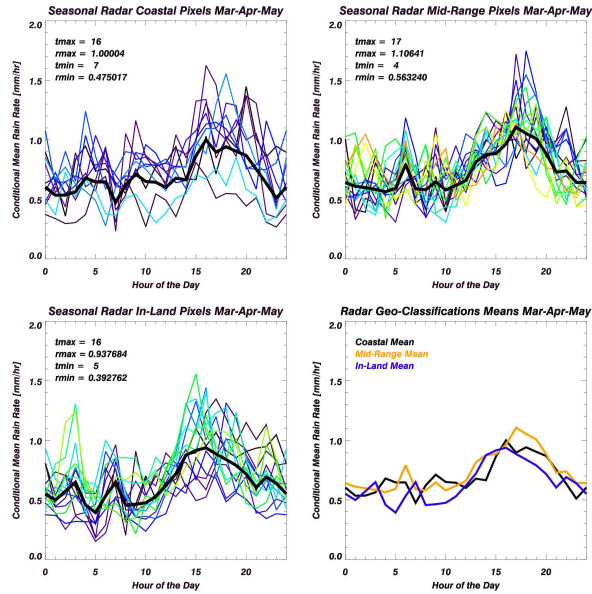


Figure 10. The spring diurnal cycle of conditional mean rain rate using radar data for the three geographical regions. The bold lines are the average of all the pixels in a given region, and are compared in the bottom right panel. These statistics were derived from the 2A-53 rain rate product over a ten year period from 2000-2009.

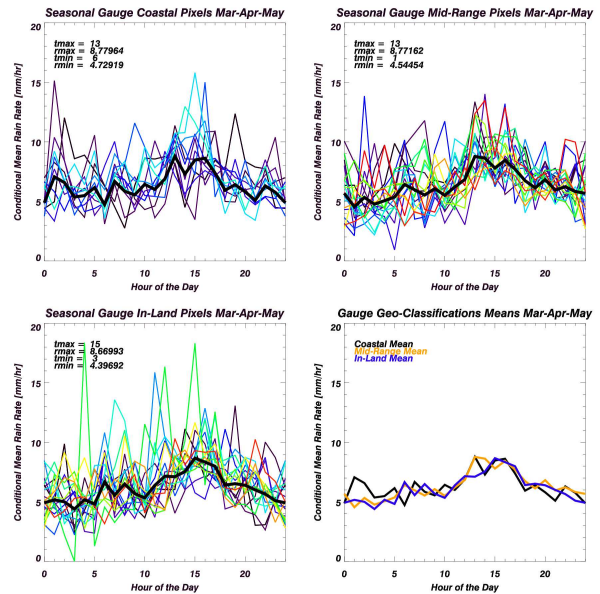


Figure 11. The spring diurnal cycle of conditional mean rain rate using gauge data for the three geographical regions. The bold lines are the average of all the pixels in a given region, and are compared in the bottom right panel. These statistics were derived from the 2A-56 rain gauge product over a ten year period from 2000-2009.

morning mode. The autumn morning mode, influenced by maritime convection that moves inland, affects the annual early and late morning modes. The most influential aspect of spring on the annual cycle is its afternoon maximum. Analysis of r_{min} reveals coastal pixels generally have the highest values for all seasons due to influences of oceanic moisture and nocturnal maritime convection. Analysis of the time that t_{max} and t_{min} occur helps illustrate how the precipitation propagates, develops, and eventually dissipates. Gauge and radar data both have similar findings though the radar data conveys a more robust result. Radar data samples the entire 27 km² grid versus point measurements within that grid for gauge data. The sparseness of gauge data as you move inland also causes a discrepancy with the radar data. A dense inland rain gauge network would provide results, possibly more consistent with radar data findings. Our observations provide crucial data for climatological validation of satellite retrievals, and will assist in the improvement of physically-based satellite retrieval algorithms.

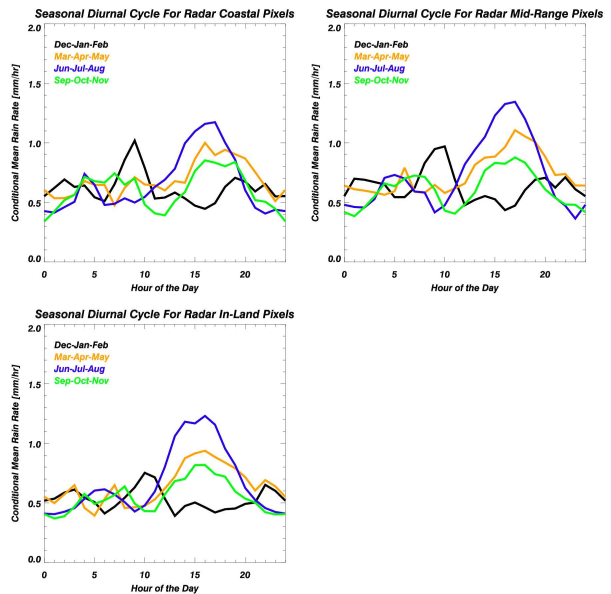


Figure 12. For radar data each seasons diurnal cycle is plotted within their region to show differences in phase and amplitude.

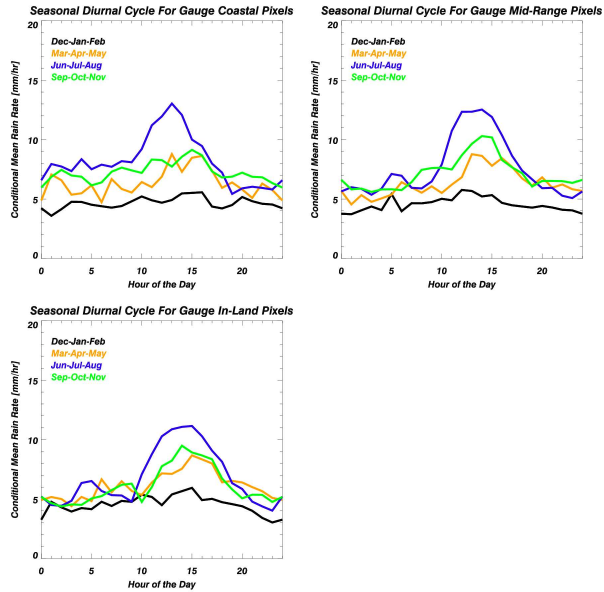


Figure 13. For gauge data each seasons diurnal cycle is plotted within their region to show differences in phase and amplitude.

8. REFRENECES

Kikuchi, K., B. Wang, 2007: Diurnal Precipitation Regimes in the Global Tropics. *J. Climate*, **21**, 2680-2696.

Mapes, B.E., T.T. Warner, M. Xu, 2002: Diurnal Patterns of Rainfall in Northwestern South America. Part III: Diurnal Gravity Waves and Nocturnal Convection Offshore. *Mon. Wea. Rev.*, **131**, 830-844.

Sorooshian, S., X. Gao, K. Hsu, R. A. Maddox, Y. Hong, H. V. Gupta, B. Imam, 2002: Diurnal Variability of Tropical Rainfall Retrieved from Combined GOES and TRMM Satellite Information. *J. Climate*, **15**, 983–1001.

Rosenfeld, D., D.B. Wolff, and E. Amitai, 1994: The Window Probability Matching Method for Rainfall Measurements with Radar. *J. Appl. Meteor.*, **33**, 682–693.

Roy, S.S., R.C. Balling, 2005: Analysis of Diurnal Patterns in Winter Precipitation across the Conterminous United States. *Mon. Wea. Rev.*, **133**, 707–711.

Schwartz, B.E., L.F. Bosart, 1979: The Diurnal Variability of Florida Rainfall. *Mon. Wea.*

Rev., **107**, 1535-1545.

Wolff, D.B., D.A. Marks, E. Amitai, D.S. Silberstein, B.L. Fisher, A. Tokay, J. Wang, and J.L. Pippitt, 2005: Ground Validation for the Tropical Rainfall Measuring Mission (TRMM). *J. Atmos. Oceanic Technol.*, **22**, 365-379.

Yang, S., and E.A. Smith, 2006: Mechanisms for Diurnal Variability of Global Tropical Rainfall Observed from TRMM. *J. Climate*, **19**, 5190–5226.